

A dynamical evolution of GRB-Afterglows in a new generic model

E Zouaoui and N Mebarki

Laboratoire de Physique Mathématique et Subatomique,
Frères Mentouri University, Constantine 1, Algeria

E-mail: esma.zouaoui213@gmail.com

Abstract. A new model using a general expression of the radiation energy and explaining the dynamics of the afterglows is proposed. It is shown that this model is suitable for the ultra-relativistic and non-relativistic phases as well as the study of radiative and adiabatic fireballs.

1. Introduction

Until now, the mystery of the gamma ray bursts (GRBs) which are the brightest and violent events in the universe after the Big Bang is still a big puzzle for astrophysicists and observers to be understood [1]. In fact, This phenomenon starts by a prompt emission of the GRBs where the energy $E \sim 10^{51} - 10^{54} \text{ergs}$, than end up with remnant emission called afterglows. At this stage scientists were able to measure the redshift [2] [3] from the obtained spectral lines, showing their cosmological origin. So far, many works were done in the literature trying to simulate this phenomenon and understand it [4] [5] [6] [7] [8] [9] [10] [11]. To be more specific the duality of fireball blast-wave model was successful where its predictions converge with data. In this model two jets explode from the core in two opposite directions, as a result they shock the surrounding medium and emit radiations where the wave lengths run from the gamma to the radio rays spectrum. In what follows we propose a GRB-afterglows hydrodynamical model taking into account the synchrotron emission as a major radiation mechanism and neglecting the absorption (such as synchrotron self-absorption) and diffusion (such as inverse Compton scattering) effects. It is very important to mention that the limitation of the earlier models [25] is related to the compatibility with the Sedov solution starting from a non-relativistic phase where we have an adiabatic processes and surrounding interstellar medium (ISM). In the present paper, as it will be shown in the next sections, the Sedov solution was satisfied achieving the energy conservation in the adiabatic regime. In section 2, we present the conventional models [12] [13] [15] then we introduce our generic new model. In section 3, we discuss our numerical results and finally in section 4, we draw our conclusions.

2. Dynamics and radiation

2.1. Conventional dynamical models

So far, in literature many models have been proposed to describe the expansion of the GRB remnants such as the one of Chiang et al of ref.[12] where:

$$\frac{d\Gamma}{dm} = -\frac{\Gamma^2 - 1}{M} \quad (1)$$

and

$$M = M_0 + m + (1 - \varepsilon)\frac{U}{c^2} \quad (2)$$

here Γ , M , m , ε and $dU = (\Gamma - 1)dmc^2$ are the Lorentz factor, the total mass of the fireball that includes the initial mass M_0 of the jet (ejected by the progenitor of the GRB), the swept mass from the external environment, the efficiency of radiation and the fraction of the internal non radiative energy, respectively. We remind that this first proposed model was written just for the relativistic phase expansion, because the solution of eq.(1) is not consistent with Sedov results for an adiabatic expansion of non relativistic phase. On the other hand, Huang et al of ref.[13] have proposed new generalized model which is more or less fairly good for ultra relativistic and non relativistic phases. In this ref.[13], the authors have used an infinitesimal difference equation for the internal non radiative energy such as $dU = d[(\Gamma - 1)mc^2]$ which was assumed and proposed by Panaitescu et al [14]. In this model, eq.(1) is replaced by the following equation:

$$\frac{d\Gamma}{dm} = -\frac{\Gamma^2 - 1}{M_0 + \varepsilon m + 2(1 - \varepsilon)\Gamma m} \quad (3)$$

where the radiation efficiency ε was assumed to be constant during the deceleration.

In 2002 Feng et al [15] [16] suggested that ε is a variable belonging to the interval [0,1] and proposed an infinitesimal difference equation for U of the form:

$$dU = d[(1 - \varepsilon)U_{ex}] \quad (4)$$

where $U_{ex} = (\Gamma - 1)mc^2$ is the internal energy produced in the expansion. In this case one has [17]:

$$\frac{d\Gamma}{dm} = -\frac{\Gamma^2 - 1}{M_0 + m + U/c^2 + (1 - \varepsilon)\Gamma m} \quad (5)$$

with:

$$\varepsilon = \varepsilon_e \frac{t'_{syn}{}^{-1}}{t'_{syn}{}^{-1} + t'_{ex}{}^{-1}} \quad (6)$$

Here

$$t'_{syn} = 6\pi m_e c / (\sigma_T B'^2 \gamma_{min}) \quad (7)$$

and

$$t'_{ex} = R / (\Gamma c) \quad (8)$$

are the synchrotron cooling and expansion times in the co-moving frame respectively. The parameters ε_e is a fraction of the internal energy carried by the accelerated electrons in the jet, m_e the rest electron mass, σ_T is the Thomson cross section and $B' = (8\pi\varepsilon_B e')^{1/2}$ the magnetic energy density where ε_B is the fraction of the kinetic energy of the shock converted into a

magnetic energy and e' an energy density defined in ref.[18]. The radius R of the blast-wave is determined by the relation [12]:

$$\frac{dR}{dt} = \beta c \Gamma (\Gamma + \sqrt{\Gamma^2 - 1}) \quad (9)$$

where $\beta = v/c$ is the jet velocity and γ_{min} the minimum Lorentz factor depending on the index p ($2 < p < 3$) and is given by [18]:

$$\gamma_{min} = \varepsilon_e \left(\frac{p-2}{p-1} \right) \left(\frac{m_p}{m_e} \right) (\Gamma - 1) + 1 \quad (10)$$

m_p being the rest proton mass.

In the highly radiative case where ($\varepsilon \simeq 1, U = 0$), eqs.(3) and (5), together with eq.(1) reduce to the following differential equation [13]:

$$\frac{d\Gamma}{dm} = -\frac{\Gamma^2 - 1}{M_0 + m} \quad (11)$$

where the analytic solution is [13]:

$$\frac{(\Gamma - 1)(\Gamma_0 + 1)}{(\Gamma + 1)(\Gamma_0 - 1)} = \frac{(m_0 + M_0)}{(m + M_0)} \quad (12)$$

with Γ_0 and m_0 are the initial values of Γ and m respectively.

In the fully adiabatic case where ($\varepsilon \simeq 0, U = U_{ex}$), eqs.(3) and (5) become [13]:

$$\frac{d\Gamma}{dm} = -\frac{\Gamma^2 - 1}{M_0 + 2\Gamma m} \quad (13)$$

leading to the analytic solution [13]:

$$(\Gamma - 1)M_0 c^2 + (\Gamma^2 - 1)m c^2 = E_{k0} \quad (14)$$

where E_{k0} is the initial value of the kinetic energy E_k .

2.2. Our generic new model

In the Feng et al model [15], and because of the behavior of the radiation efficiency ε evolving with time, a differential equation for the internal residual energy in the fireball for the dynamical evolution of the GRB-afterglows was proposed. However the change in the radiative part was ignored.

In fact the total kinetic energy E_k of the fireball is given by [14]:

$$E_k = (\Gamma - 1)(M_0 + m) + \Gamma U \quad (15)$$

The global conservation of energy implies that:

$$dE_k = -dE_{rad} \quad (16)$$

where dE_{rad} is the radiative part from the internal energy of the fireball. The definition given by Blandford et al is $dE_{rad} = \varepsilon \Gamma (\Gamma - 1) dm c^2$ [19]. The internal energy created within the fireball is U_{ex} , such that:

$$dE_{rad} = \varepsilon \Gamma dU_{ex} \quad (17)$$

This due to the fact that the internal energy can be radiative or remains in the fireball and has the same form up to a factor ε (resp. $1 - \varepsilon$) for radiative (resp. residual) internal energy. Therefore, eq.(17) can be rewritten as:

$$dE_{rad} = \varepsilon\Gamma[(\Gamma - 1)dm + m d\Gamma]c^2 \quad (18)$$

Using eqs. [(15)- (18)], one obtains the following differential equation describing the evolution of the fireball and consistent with the Sedov solution.

$$\frac{d\Gamma}{dm} = -\frac{\Gamma^2 - 1}{M_0 + m(\Gamma + 1) + U/c^2} \quad (19)$$

It is important to notice that in the adiabatic case when $\varepsilon \simeq 0$, eq.(19) reduces to eq.(13) while in the highly radiative case where ($\varepsilon \simeq 1$) eq. (19) gets the new form:

$$\frac{d\Gamma}{dm} = -\frac{\Gamma^2 - 1}{M_0 + m(1 + \Gamma)} \quad (20)$$

leading to the following analytic solution:

$$\Gamma = -1 + \frac{M_0}{m} \text{productLog} \left[\frac{m}{M_0} e^{\frac{2m-C}{M_0}} \right] \quad (21)$$

(C is an integration constant)

Moreover, it was show that the total luminosity of the fireball has the following form:

$$L = L_B + \Gamma\varepsilon mc^2 \frac{d\Gamma}{dt} \quad (22)$$

where L_B is the total luminosity used in the models of refs.[15] [13] and has as expression $L_B = \Gamma\varepsilon[(\Gamma - 1)c^2 dm/dt]$ and Γ is giving by eq. (21).

2.3. Synchrotron radiation

The distribution of the accelerated electrons by the external shock behind the blast wave in the absence of the radiation loss is generally assumed to be a power-law function of the electron energy [17]:

$$N'_e(\gamma_e) = \frac{dN'_e}{d\gamma_e} = C t^e \gamma_e^{-P}, \gamma_{min} \leq \gamma_e \leq \gamma_{max} \quad (23)$$

where $\gamma_{max} = a10^7(B'/1G)^{-1/2}$ ref.[19] is the maximum Lorentz factor and "a" is a factor taking its values between 1 and 10. The power for synchrotron radiation $P_{\nu'}$ is defined as [18]:

$$P_{\nu'} = \frac{2\sqrt{3}e^2\nu_L}{c} \int_{\gamma_{min}}^{\gamma_{max}} N'_e(\gamma_e) F\left(\frac{\nu'}{\nu'_c}\right) d\gamma_e \quad (24)$$

where F(x) is the synchrotron function such that [20]:

$$F(x) = x \int_x^{\infty} K_{5/3}(x') dx' \quad (25)$$

Here $K_{5/3}$ is the second kind modified Bessel function. The synchrotron frequency given ν'_c by [22]:

$$\nu'_c = \frac{2}{3}\nu_L\gamma_e^2 \quad (26)$$

where ν_L is the Lamor frequency:

$$\nu_L = \frac{1}{2\pi} \frac{eB'}{2m_e c} \quad (27)$$

Notice that the radiation in the lab frame can be calculated using the relativistic transformations [21] [22]:

$$\nu = \frac{(1 + \beta)\Gamma}{1 + z} \nu' \quad (28)$$

where z is the redshift.

The instantenous intensity F_ν giving the light curves at a frequency ν in Jansky ($erg.s^{-1}.cm^{-3}.Hz^{-1}$) is:

$$F_\nu = \frac{1}{4\pi D_L(z)^2} 4\pi \frac{dP_\nu}{d\Gamma} \quad (29)$$

where $D_L(z)$ is the luminosity distance in the Λ CDM model with $\Omega_M = 0.3, \Omega_\Lambda = 0.7$ and $H_0 = 71 km.s^{-1} Mpc^{-1}$. Note that for observations by satellites or terrestrial telescopes one has to use S_B by integrating F_ν in a giving interval $[\nu_1, \nu_2]$:

$$S_B = \int_{\nu_1}^{\nu_2} F_\nu d\nu \quad (30)$$

3. Numerical results and discussion

The variation of the mass swepted by the fireball during the deceleration is given by:

$$dm = 4\pi R^2 n m_p dR \quad (31)$$

where

$$dR = \beta c \Gamma (\Gamma + \sqrt{\Gamma^2 - 1}) dt \quad (32)$$

here t is the observed time and measured by telescopes and satellite. In solving eqs. (1), (3), (5) and (19) numerically, the initial parameters are taken as: $\Gamma_0 = 250, M_0 = 2.10^{-6} M_\odot, p = 2.1, \theta = 10^\circ$ (solid angle parameters), $a = 4.0$ and $g = 0$ with $k = 0, n = 1 cm^{-1}$ corresponding to the interstellar medium (ISM) ref.[25].

Fig.1 displays the evolution of the jet velocity calculated according to eqs. (3), (5) and (19) [23]. Notice that the three models are compatible with the Sedov solution, in the non relativistic (NR) limit for the adiabatic case [24], where the velocity is proportional to $R^{-3/2}$. However in the other regions the solution of eq.(19) is different from those of eqs. (3), (5). In fact for the ultra relativistic (UR) case where $x = m/M_0 \ll 1$, the principal branch of Lambert productlog(z) function denoted by $W_0(z)$ with $z = x e^{2x-C}$ (C is integration constant) has the following series expansion near $\frac{1}{e}$ (e: exponential) as $W_0(x) \approx -1 + \sqrt{2(ex+1)} + o(\sqrt{x+\frac{1}{e}})$ which leads to $\Gamma \approx \frac{-1+e}{\sqrt{2}} + \frac{\sqrt{2}-1}{x} + \mathcal{O}(\sqrt{x+\frac{1}{e}}) \sim \frac{\sqrt{2}-1}{x} \sim R^{-3}$. Of course in this limit $\beta \rightarrow 1$ one can explain the almost horizontal curve in the region of interval $R \in [10^{14} - 10^{18}] cm$, although there is a small shift due to the fact that in our model $\beta = 1 - \frac{1}{\Gamma^2} \approx 1 - \frac{2x}{\sqrt{2}-1}$. For the non relativistic case where $x \gg 1$ or equivalently $z \gg 1$ or $R \in [10^{19} - 10^{23}] cm$ in the region of an interest the $W_0(z)$ function has the following series expansion $W_0(z) \approx \ln z - \ln \ln z + \frac{\ln \ln z}{\ln z} + o(\frac{\ln \ln z}{\ln z})$ $\Gamma = -1 + \frac{M_0}{m} productLog[\frac{m}{M_0} e^{2\frac{m}{M_0}-C}]$. Notice that in our model if $x \gg 1$, $\Gamma \approx 1 - \frac{c+\ln 2}{x} \sim -\frac{c+\ln 2}{x} \sim R^{-3}$ (numerical result shows that $c \ll -\ln 2$) leading to $\beta \sim R^{-\frac{3}{2}}$ instead of $\beta \sim R^{-3}$ ref.[13]-[15]. This explains the difference slope (in logarithmic scale between our model and that of ref. [13]-[15] In fact in our new model the slope is smaller than that of ref.[13]-[15]).

Similar behaviors are noticed in fig.2 where the evolution of the Lorentz factor for the radiative case shows a faster drop (large slope) in our new model. Furthermore the curve of the three mentioned models coincide in the non-relativistic region. In fact in fig.2 (see the curve in UR limit), in the adiabatic case where $\epsilon = 0$ and in all models we obtain the same differential eq.(13) which has as a solution eq.(14) and therefore in the UR (resp NR) limit $\Gamma \sim R^{-\frac{3}{2}}$ (resp $\beta \sim R^{-\frac{3}{2}}$) since $m \sim R^3$. For the radiative case where $\epsilon = 1$, in our model we end up with the differential equation $\frac{d\Gamma}{dm} = -\frac{\Gamma^2-1}{M_0+m(\Gamma+1)}$ which has as a solution $\Gamma = -1 + \frac{M_0}{m} \text{productLog}[\frac{m}{M_0} e^{2\frac{m}{M_0}-C}]$. In the UR limit $\Gamma \approx (\sqrt{2}-1)\frac{M_0}{m} + \frac{e-1}{\sqrt{2}} \sim \frac{M_0}{m} \sim R^{-3}$. However in the NR limit one gets $\Gamma \sim 1 - (C + \ln 2)\frac{M_0}{m}$ (~ 1) and $\beta \sim \sqrt{-2\frac{C+\ln 2}{x}} / (1 - \frac{C+\ln 2}{x}) \sim x^{-\frac{1}{2}} \sim R^{-\frac{3}{2}}$.

It is worth to mention that, in the other models of ref. [13]-[11], one has a different differential equation that is $\frac{d\Gamma}{dm} = -\frac{(\Gamma^2-1)}{M_0+m}$ which has as a solution $\frac{(\Gamma-1)(\Gamma_0+1)}{(\Gamma+1)(\Gamma_0-1)} = (\frac{m_0+M_0}{m+M_0})^2$ where m_0 is the initial mass. It is obvious that in the UR limit $\Gamma \sim \frac{M_0}{m} - 1 \sim R^{-3}$ and in the NR limit $\beta \sim R^{-3}$ (difference in power of R in comparison to our model). Again, the difference in the slope of Γ as a function of R (in a logarithmic scale) is due essentially to the fact that we do not have the same solution of the two different differential equations mentioned above. Finally, in the NR limit, $\Gamma \rightarrow 1$ that is why all curves tends to the same limit.

Fig.3 shows the total kinetic energy E_k as a function of R. Notice that for the case $\epsilon \simeq 1$. E_k decreases slower in our new model than the proposed others models [13] [15] and it is almost flat in the range of $R \simeq 10^{16} - 10^{17} \text{ cm}$ (UR) and $R \simeq 10^{18} - 10^{19} \text{ cm}$ (NR). In the adiabatic case E_k is constant for all the models ($E_k \sim 10^{51} \text{ erg}$).

Fig.3 displays the evolution of the total kinetic energy E_k as a function of the distance R in a logarithmic scale for both the radiation and adiabatic cases where $\epsilon = 1$ and $\epsilon = 0$ respectively. In fact we remaind that when $\epsilon = 0$ for all models (including ours), the solution of eq.(13) is that given by eq.(14) leading to $E_k = E_{k_0} = (\Gamma - 1)M_0c^2 + (\Gamma^2 - 1)mc^2 = C^{te}$ This explains why the kinetic energy is constant in dependently of the variation of R (both in the NR or UR cases). However, for $\epsilon = 1$ (radiative case), the situation is different, especially in the NR case. The reason lies in the fact that eq. (21) reduces to $\Gamma \sim 1 - (C + \ln 2)\frac{M_0}{m}$ (as it was pointed out earlier) than the expansion of the kinetic energy $E_k = (\Gamma - 1)M_0c^2$ (common to all models when $\epsilon = 1$) will be $\sim -(C + \ln 2)\frac{M}{m}(M + M_0)$ and since $m \ll \gamma_0 M_0$ than $E_k \sim -(C + \ln 2) = C^{te}$. For the other models, using eq.(12) we deduce that $E_k \sim 2 \frac{(m_0+M_0)^2(\Gamma_0-1)}{(\Gamma_0+1)} \frac{1}{m+M_0} \sim \frac{1}{m} \sim R^{-3}$. In the logarithmic scale, this behaves like a straight line with a slope = -3. For the UR case, our model gives using eq.(12) and $\Gamma \sim \frac{\sqrt{2}-1}{m}M_0 \sim \frac{1}{m} \sim R^{-3}$, $E_k \sim \frac{\Gamma}{m+M_0} \sim \frac{\Gamma}{M_0} \sim R^{-3}$. Similar expressions can be obtained for the other models. Notice in this case we have the same behavior of E_k as a function of R expect of course the proportionality factor a small shift due the difference of the solution of Γ between our model and the others.

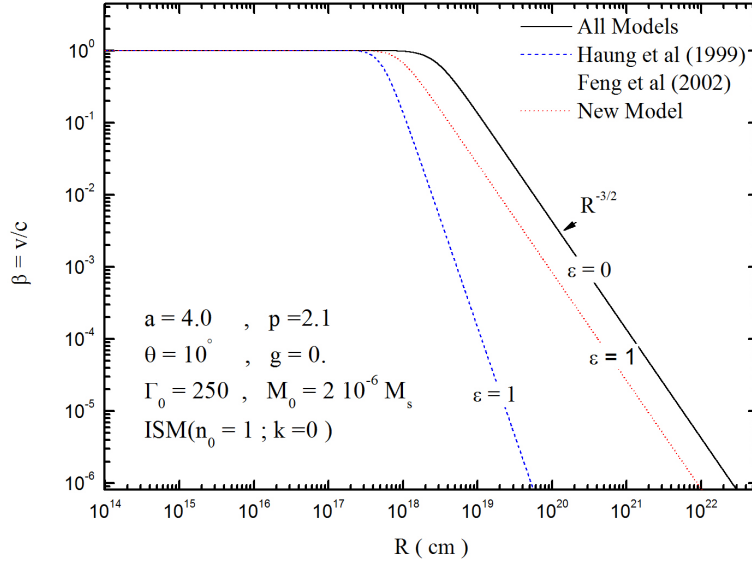


Figure 1. Evolution of the jet velocity $\beta = v/c$ as a function of the distance R (in logarithmic scale). For radiative ($\varepsilon = 1$) and adiabatic ($\varepsilon = 0$) cases.

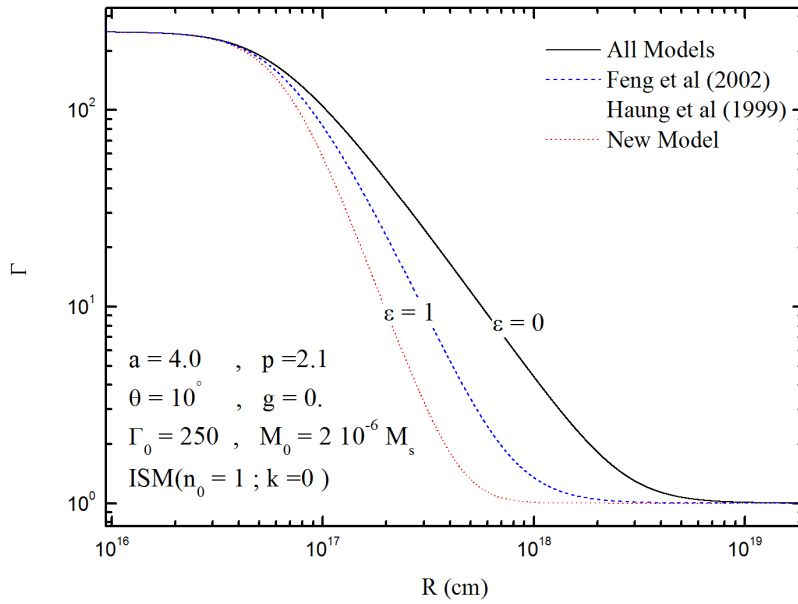


Figure 2. Evolution of the Lorentz factor Γ as a function of the distance R (in logarithmic scale). For radiative ($\varepsilon = 1$) and adiabatic ($\varepsilon = 0$) cases.

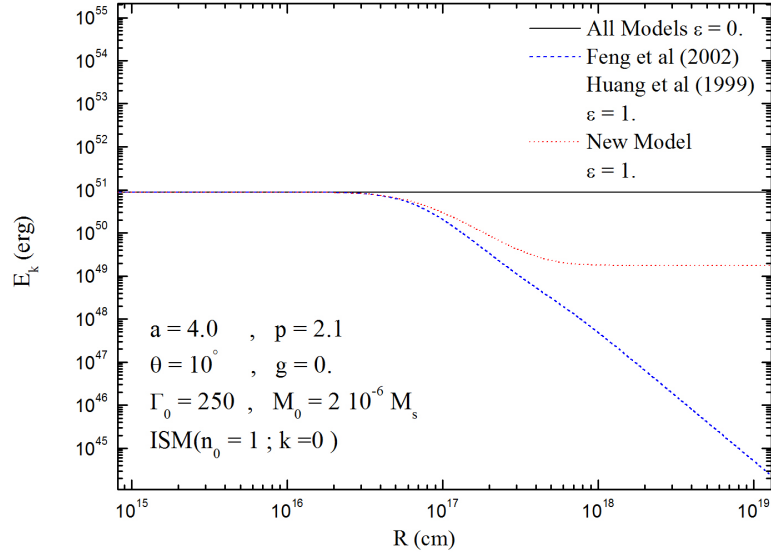


Figure 3. Evolution of the total kinetic energy E_k as a function of the distance R (in a logarithmic scale). For radiative ($\varepsilon = 1$) and adiabatic ($\varepsilon = 0$) cases.

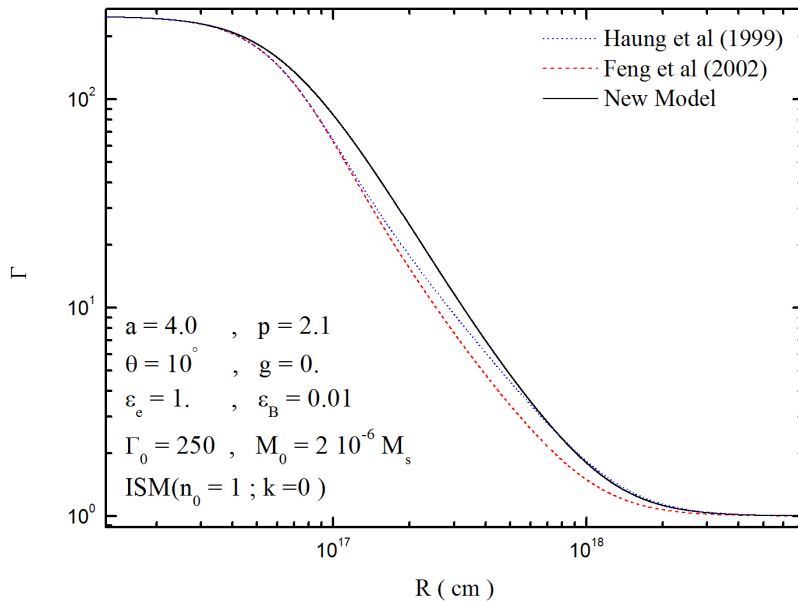


Figure 4. Evolution of the Lorentz factor Γ as a function of the distance R (in logarithmic scale). For $\varepsilon_e = 1$ and $\varepsilon_B = 0.01$.

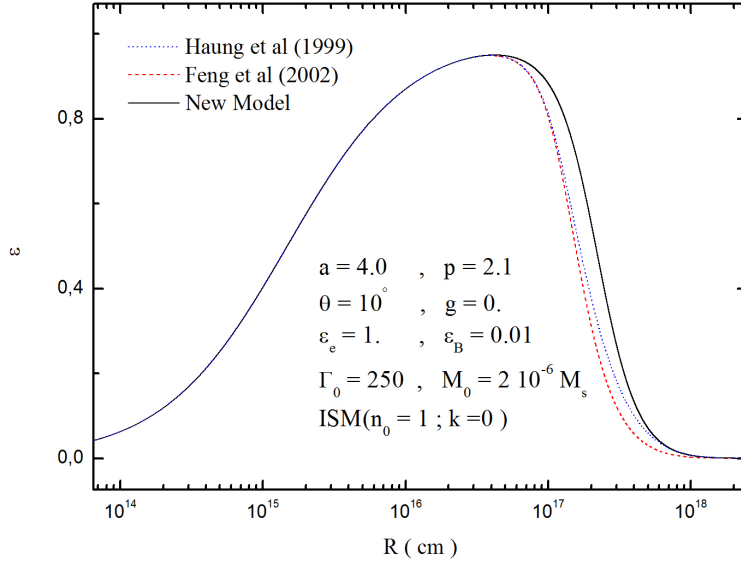


Figure 5. Evolution of the radiative efficiency of the fireball ε as a function of the distance R (in logarithmic scale). For $\varepsilon_e = 1$. and $\varepsilon_B = 0.01$.

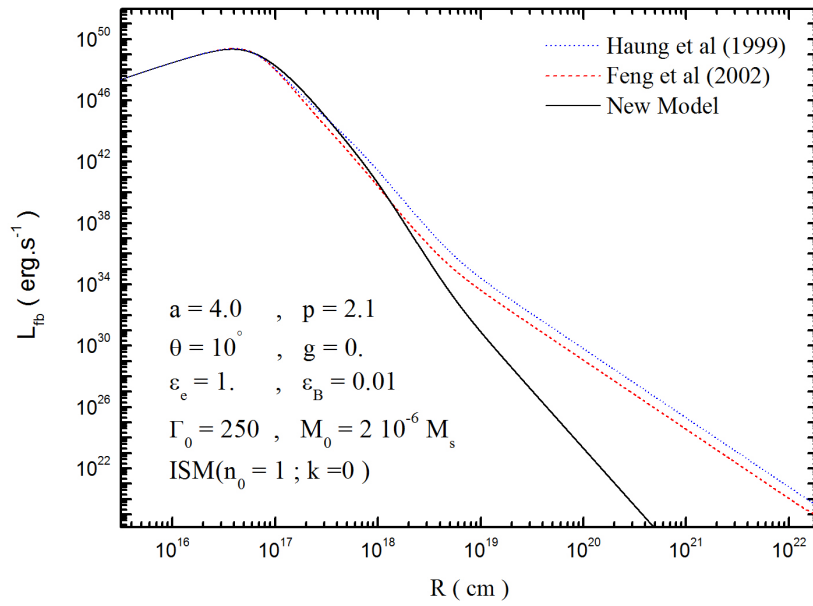


Figure 6. Evolution of the total luminosity of the fireball L_{bf} as a function of the distance R (in logarithmic scale). For $\varepsilon_e = 1$. and $\varepsilon_B = 0.01$.

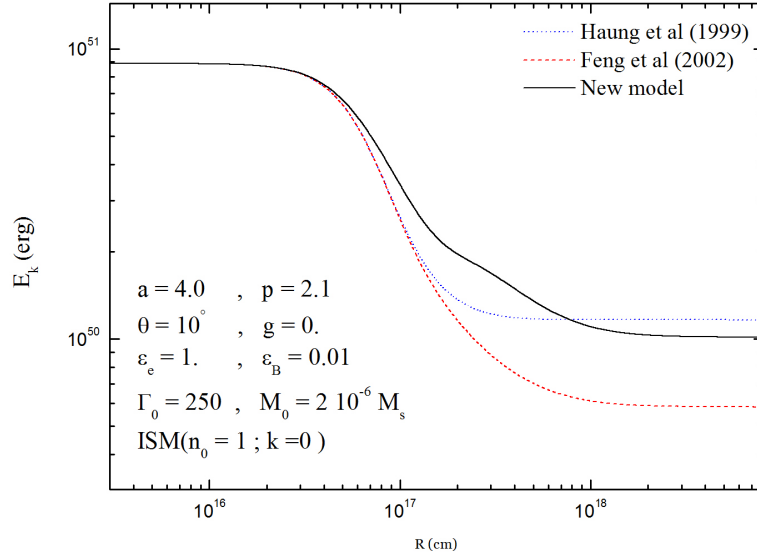


Figure 7. Evolution of the total kinetic energy E_k as a function of the distance R (in logarithmic scale). For $\varepsilon_e = 1.$ and $\varepsilon_B = 0.01.$

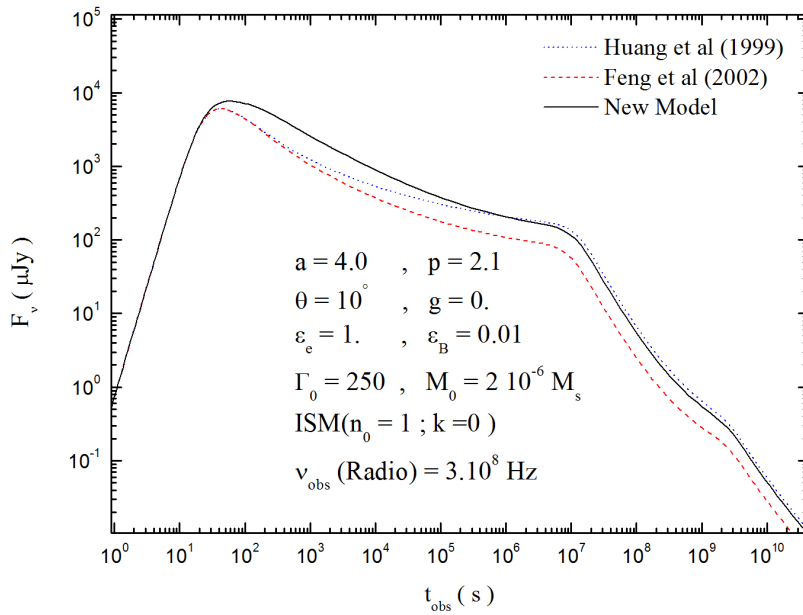


Figure 8. Light curve of GRB Afterglow (in logarithmic scale) within Huang et al (1999), Feng et al (2002) and the new models for radio frequency $\nu_{\text{obs}} = 3.10^8 \text{ Hz}.$

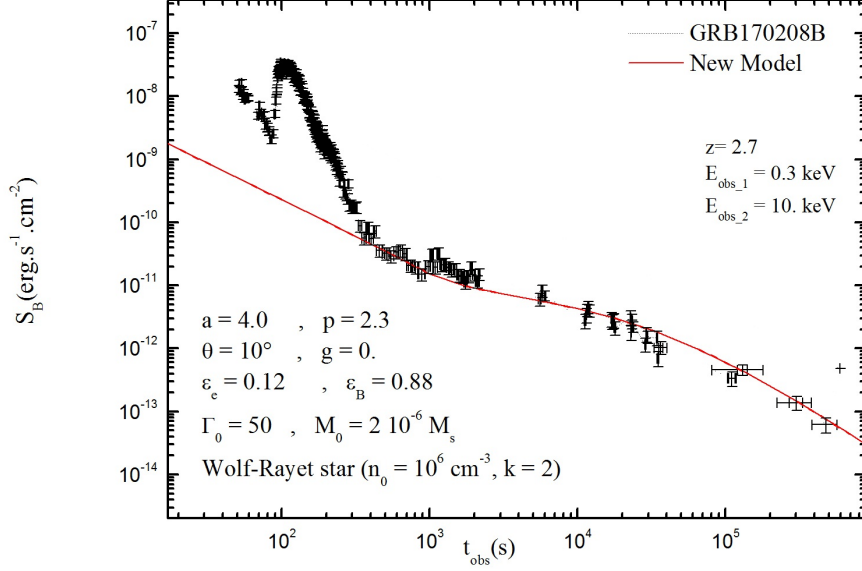


Figure 9. Integrated light curves of the GRB170208B Afterglow observed by the XRT / Swift telescope and their simulation (in logarithmic scale).

Fig.5 shows the evolution of the radiative efficiency of the fireball ϵ as a function of the distance R for our model (black solid line), Feng et al model (red dashed line) and Huang et al (blue dashed line) for $\epsilon_e = 1$ and $\epsilon_B = 0.01$. Notice that our curve is a little bit shifted in the interval $10^{17} - 10^{18} cm$, and coincide in the region where $R > 10^{18} cm$. Notice also in comparison with other models the maximum which appears at $R \sim 5 \times 10^{16} cm$. For $R \gg$ (NR case) the three curves coincide (similarly for the UR case). For the intermediate values of R , the efficiency ϵ in our model is bigger than that of the Feng and Huang models for the same radius R . For example for $R \sim 210^{17} cm$, $\epsilon_{ourmodel} \approx 0.49$, $\epsilon_{Huang} \approx 0.37$ and $\epsilon_{Feng} \approx 0.27$. To justify this behavior, we notice that using eqs. (7) and (8) defining t'_{syn} and t'_{ex} respectively, eq. (6) takes the form $\epsilon = \epsilon_e [1D\Gamma R^{-1}(A\Gamma + B)^{-1}(\Gamma - 1)^{-2}]^{-1}$ where A , B and D are constants. Now in the NR region where R is large and $\Gamma \simeq 1$, $\epsilon \rightarrow \epsilon_e = 1$ (see our figure). However in the UR region where Γ is larger $\epsilon \rightarrow \epsilon_e \frac{A\Gamma^2\Gamma}{A\Gamma^2 + D}$ and this is a decreasing function of $R\Gamma^2$. Our numerical results show that $\frac{d\Gamma}{dt} = \frac{d\Gamma}{dR} \frac{dR}{dt}$ is a decreasing function of R and since $\frac{d\Gamma}{dt} \sim \Gamma^2$ (for a larger value of Γ see eq.(9)) then $\frac{d\Gamma}{dR}$ decreases faster than $\frac{1}{\Gamma^2}$ as a function of R and consequently ϵ is a decreasing function of R as it is shown in fig.5. Now, the shift of ϵ in our model compared to the others, lies in the fact that numerical results show that within the interval of $R \in [10^{16}, 10^{19}]$, the Lorentz factor Γ of our model is greater than that of ref. [13]-[15] for a fixed value of R (see figure 4) or equivalently for a fixed value of Γ . The radius R of our model is greater than that of ref. [13]-[15]. Therefore if eq.(6) is rewritten as $\epsilon = \epsilon_e \frac{1}{D\Gamma/R(A\Gamma+B)(\Gamma-1)^2}$, than it is obvious that if $R_{ourmodel}$ is greater than $R_{othermodels}$ (for a fixed value of Γ), one has $\epsilon_{ourmodel} > \epsilon_{othermodels}$.

Fig.6 displays the luminosity as a function of the radius R . Notice that there is a concordance between the three models in the range $10^{15} - 10^{18} cm$ than the curve becomes steeper in our model in the range $> 10^{19} cm$.

Fig.6 shows the luminosity L_{bf} as a function of R for a variable efficiency ϵ . Notice

that L is a decreasing function of R and for relatively smaller values of R (UR case) it is almost of the same order (for our model and those of ref. [13] [15]) with a small shift difference (ours is larger). For example for $R = 10^{16}cm$, $L_{ourmodel} \approx 1.4410^{49}erg.s^{-1}$ and $L_{Feng} \approx L_{Huang} \approx 910^{48}erg.s^{-1}$. Now, if R increases, $L_{ourmodel}$ decreases faster than L_{Feng} and L_{Huang} for example for $R = 10^{19}cm$, $L_{ourmodel} \approx 10^{30}erg.s^{-1}$ and $L_{Feng} \approx 3.1310^{33}erg.s^{-1}$ and $L_{Huang} \approx 1.9210^{34}erg.s^{-1}$. Therefore, for larger values of R (NR case), the discrepancy increases between the results of our model and those of ref. [13] [15]. This is due mainly to the fact that L contains two compelling terms $L_1 = \Gamma\varepsilon(\Gamma - 1)\frac{dm}{dt}$ which is positive and $L_2 = \Gamma\varepsilon m\frac{d\Gamma}{dt}$ (present only in our model), which is negative. As R increases, L_2 increases and compensates L_1 , such that $L = L_2 + L_1$ become smaller in comparison with the other models where the term L_2 is absent. Table 1, summarizes some numerical values illustrating this fact.

R(cm)	$L_1(erg.s^{-1})$			$L_2(erg.s^{-1})$	$L_1 + L_2(erg.s^{-1})$
	Huang	Feng	Our model		
1.09×10^{16}	3.48785×10^{48}	3.48786×10^{48}	3.48798×10^{49}	-1.5353×10^{46}	3.47263×10^{48}
1.13×10^{17}	5.5×10^{47}	4.29×10^{47}	2.09×10^{48}	-1.16×10^{48}	9.36×10^{47}
1.03×10^{18}	2.5×10^{41}	2.0×10^{40}	1.71×10^{41}	-1.40×10^{41}	3.08×10^{40}
1.06×10^{19}	1.92×10^{34}	3.13×10^{33}	1.3323×10^{34}	-1.3318×10^{34}	5.01×10^{30}
1.10×10^{20}	4.29×10^{29}	7.63×10^{28}	3.03813×10^{29}	-3.03812×10^{29}	1.04×10^{23}

Table 1. Some numerical results illustrating the luminosity of the three models

Fig.7 displays the total kinetic energy E_k as a function of the distance R . For $\varepsilon_e = 1$. and $\varepsilon_B = 0.01$. Notice the discrepancy between the three models for the range $> 5 \times 10^{16}cm$. The curves in the three models became almost flat in the region $R > 10^{18}cm$. Notice also the existence of tow slopes in our new model in the region $R > 5 \times 10^{16} - 10^{18}cm$.

Fig.7 displays E_k as a function of R . Notice that for values of $R = 10^{16}cm$ (UR region), E_k takes almost the same value for the three models ($E_k \approx 8.86 \times 10^{50}erg$). The reason lies to the fact that in the UR region where Γ is larger and $M_0 \gg m$, $\varepsilon \approx \varepsilon_e$ (see eq.(6)) and therefore in all models we have $E_k \sim (\Gamma - 1)M_0$ and almost the same differential equation $\frac{d\Gamma}{dm} = -\frac{\Gamma^2-1}{M_0}$. In the NR region where $m \gg M_0$ and $\Gamma \approx 1$, E_k becomes constant. For example for $R \approx 10^{19}cm$, $E_{k(Huang)} \approx 1.16 \times 10^{50}erg$, $E_{k(Feng)} \approx 6.09 \times 10^{49}erg$ and $E_{k(Ourmodel)} \approx 1.07 \times 10^{50}erg$ and $R \approx 10^{20}cm$, $E_{k(Huang)} \approx 1.15 \times 10^{50}erg$, $E_{k(Feng)} \approx 5.79 \times 10^{49}erg$, $E_{k(Ourmodel)} \approx 1 \times 10^{50}erg$, (see table 2). The reason lies to the fact that, in the NR region where $\Gamma \approx 1$, $\varepsilon \approx 0$ and $U \approx m(\Gamma - 1) + c^{te}$, one has $\frac{d\Gamma}{dm} \sim -\frac{\Gamma^2-1}{M_0}$ for all models which leads to $m \sim \frac{1}{\Gamma-1}$ and therefore $E_k \approx 2(\Gamma - 1)m + C^{te}$ becomes constant. The difference in the constant between the three models is due to the complicated expression of $\varepsilon \approx \varepsilon_e \times 1/[R(A\Gamma + B)(1 - \Gamma)^2]$ (if $\Gamma \rightarrow 1$, where Γ is a function of m or equivalently R because slightly different our model to an other. Any way, numerical results shows that in the NR case, E_{Huang} becomes slightly bigger than ours and almost twice that of Feng and al. In the intermediate region where $R \approx 3 \times 10^{17}cm$; $E_{Ourmodel} \approx 1.68 \times 10^{50}cm$, $E_{Feng} \approx 8.81 \times 10^{49}cm$ and $E_{Huang} \approx 1.22 \times 10^{50}cm$. In fact, the difference between our model and Feng et al [15] (resp. Huang et al [13]) is due to the difference in the expression of the used differential equation $\frac{d\Gamma}{dm}$ (see eqs. (3) and (5)) (resp. to the difference in the experience of E_k (see eq.(15))and U (see eq.(4) and $U = U_{ex} = (\Gamma - 1)mc^2$). Table 2, summarizes the behavior of E_k in various regions.

R(cm)	E_k (erg)		
	Huang	Feng	Our model
10^{16}	8.86×10^{50}	8.86×10^{50}	8.86×10^{50}
10^{17}	2.63×10^{50}	2.59×10^{50}	3.40×10^{50}
3×10^{17}	1.22×10^{50}	8.81×10^{49}	1.68×10^{50}
10^{18}	1.16×10^{50}	5.09×10^{49}	1.07×10^{50}
10^{19}	1.16×10^{50}	5.83×10^{49}	1.01×10^{50}
10^{20}	1.15×10^{50}	5.79×10^{49}	1.00×10^{50}

Table 2. Some numerical results illustrating the kinetic energy of the three models

t_{obs} (s)	F_ν (μJy)		
	Huang	Feng	Our model
10	789.42	789.44	789.98
43	6045	6049	7333
1.2×10^3	1112	890	3159
10^6	205	98	207
10^8	6	1	4
10^9	0.6	0.2	0.4
10^{10}	0.05	0.01	0.04

Table 3. Some numerical results illustrating the instantaneous intensity of light curve of the three models

Fig.8 shows the light curve of GRB Afterglow within all model for a radio frequency $\nu_{obs} = 3.10^8 Hz$. Notice the same behavior of the three models with a small shift in comparison with Feng when $R \leq 10^2 cm$. Notice also that:

- 1) F_ν is a decreasing function of t as it is expected.
- 2) There are five regions where the slope $\frac{dF_\nu}{dt}$ change its direction. This is due to the complicated behavior of $\frac{dP}{dt}$ as a function of t.
- 3) There is a maximum (for all models) around $t \sim 43s$ ($F_{\nu(Huang)} \approx 6045 erg.s^{-1}.cm^{-2}$, $F_{\nu(Feng)} \approx 6049 erg.s^{-1}.cm^{-2}$, $F_{\nu(Ourmodel)} \approx 7333 erg.s^{-1}.cm^{-2}$). This can be explained by the fact that the synchrotron function $K(x)$ has a maximum around $x \approx 0.3$ and therefore F_ν should has a maximum corresponding approximately to $t \approx 43s$
- 4) For relatively small values of t (region 1, $t \sim 10s$), one has almost the same values of F_ν for qll models. That is: $F_{\nu(Huang)} \approx 789.42 erg.s^{-1}.cm^{-2}$, $F_{\nu(Feng)} \approx 789.44 erg.s^{-1}.cm^{-2}$, $F_{\nu(Ourmodel)} \approx 789.98 erg.s^{-1}.cm^{-2}$.
- 5) In the region 2 (where $\frac{dF_\nu}{dt}$ change the direction), our F_ν is above and different from that of Huang et al and Feng et al. For example for $t \sim 1.2 \times 10^3 s$ $F_{\nu(Huang)} \approx 1112 erg.s^{-1}.cm^{-2}$, $F_{\nu(Feng)} \approx 890 erg.s^{-1}.cm^{-2}$, $F_{\nu(Ourmodel)} \approx 3159 erg.s^{-1}.cm^{-2}$
- 6) In the region 3 where $t \sim 10^6 s$ and $F_{\nu(Huang)} \approx 250 erg.s^{-1}.cm^{-2}$, $F_{\nu(Feng)} \approx 98 erg.s^{-1}.cm^{-2}$ and $F_{\nu(Ourmodel)} \approx 207 erg.s^{-1}.cm^{-2}$, $\frac{dF_\nu}{dt}$ changes again its direction (decreases).

- 7) In the region 4 where F_ν drops faster (a more pronounced slope is noticed) $t \sim 10^8 - 10^9 s$ and $F_{\nu(Huang)} \in [6, 0.6] erg.s^{-1}.cm^{-2}$, $F_{\nu(Feng)} \in [1, 0.2] erg.s^{-1}.cm^{-2}$ and $F_{\nu(Ourmodel)} \in [0.4, 0.04] erg.s^{-1}.cm^{-2}$.
- 8) In the region 5 where $t \geq 10^{10} s (R \approx 10^{19} cm)$ and $F_{\nu(Huang)} \leq 0.05 erg.s^{-1}.cm^{-2}$, $F_{\nu(Feng)} \leq 0.01 erg.s^{-1}.cm^{-2}$ and $F_{\nu(Ourmodel)} \leq 0.04 erg.s^{-1}.cm^{-2}$, F_ν changes again its slope (increases).

Notice that in all region 1,2 and 3 in our model F_ν is above and almost the same as that of Huang et al but slightly different (almost a constant) from that of Feng et al.

Fig.9 displays the light curves of the GRB170208B Afterglow observed by the XRT / Swift telescope and their simulation. Notice the fairly good agreement of our model in the X-Ray Afterglows region $t_{obs} \geq 3 \times 10^2 s$ and this confirm the viability of our model.

4. Conclusion

Throughout this paper, a new generic model of the GRB Afterglows which verifies the Sedove solution and energy conservation in the adiabatic regime is constructed. We have studied and discussed the evolution of the jet velocity, Lorentz factor, kinetic energy, efficiency radiation coefficient, luminosity and instantenous intensity of light curve as a function of the radius of the blast wave R and/or time t. We have considered both the radiative and adiabatic cases as well as constant and variable efficiency radiation coefficient ϵ . The results f our model are compared with those of Huang et al and Feng et al models. It turns out that the behaviors and/or numerical results are almost the same in the ultra relativistic region and different globally in the other region (relativistic and non relativistic). Finally, fairly good concordance with the observational data of XRT/Swift telescope concerning the integrated light curves of the GRB170208B was obtained in the interval of our interest $t_{obs} \geq 3 \times 10^2 s$.

5. Acknowledgments

We are very grateful to the Algerian Minister of Higher Educations and Scientific Research and DGRET for the financial support.

References

- [1] Klebesadel R W, Strong I B and Olson R A 1973 *Astrophys. J. Lett.* **L85** 182
- [2] Costa E, Frontera F, Heise J, Feroci M, in't Zand J, Fiore F, Cinti M N, ... Piro L and Butler R C 1997 *Nature* **387** 783
- [3] Metzger, M R, Djorgoski S G, Steidel C C, Kulkarni S R and Frail D A 1997 *Nature* **387** 878
- [4] Shaviv N J and Dar A 1995 *Mon. Not. Roy. Astron. Soc* **277** 287
- [5] Sari R and Piran T 1997 *Astrophys. J.* **485** 270
- [6] Dermer C D and Mitman K E 1999 *Astrophys. J.* **513** L5
- [7] Kumar P 1999 *Astrophys. J.* **523** L113
- [8] Rees M J and Mészáros P 1994 *Astrophys. J. Lett.* **430** L93
- [9] Blinnikov S I, Novikov I D, Perevodchikova TV and Polnarev A G 1984 *Soviet. Astron. Lett.* **10** 177
- [10] Katz J I 1994 *Astrophys. J.* **432** 107
- [11] Rees J M and Mészáros P 1992 *Mon. Not. Roy. Astron. Soc* **P258** 41
- [12] Chiang J and Dermer C D 1999 *Astrophys. J.* **512** 699
- [13] Huang Y F, Dai Z G, and Lu T 1999 *MNRAS* **309** 513
- [14] Panaitescu A, Mészáros P and Rees J M 1998 *Astrophys. J.* **503** 315
- [15] Feng J B, Huang Y F, Dai Z G, and Lu T 2002 *Chin. J. Astron. Astrophys* **2** 525
- [16] Zouaoui E, Fouka m and Ouichaoui S 2015 *Sciences and Technologie A* **41** 71
- [17] Dai Z G, Huang Y F and Lu T 1999 *Asrophys. J.* **520** 634
- [18] Huang Y F, Dai Z G, and Lu T 1998 *Astronomy Astrophysics* **336** L68
- [19] Sari R, Piran T and Narayan R 1998 *Astrophys. J. Lett.* **497** L17
- [20] Blandford R D and MeKee C F 1976 *Phys. Fluids.* **19** 1130
- [21] Abramowitz M and Stegun I A 1965 *Handbook of Mathematical Function* (New York: Dover)

- [22] Rybicki G B and Lightman A P 1979 *Radiative Processes in Astrophysics* (New York: Wiley)
- [23] Lind K R and Blandford R D 1985 *Astrophys. J.* **295** 358
- [24] Zouaoui E Fouka M and Ouichaoui S 2011 2010 *Proc. Int. Conf on Algerian Astronomy and Astrophysics (Constantine Algeria)* vol 1444 (American Institute of Physics) p 359
- [25] Sedov L 1969 *Similarity and Dimensional Methods in Mechanics* (New York: Academic)